Dalton Transactions

PAPER

View Article Online
View Journal | View Issue

Cite this: *Dalton Trans.*, 2016, **45**, 1998

Synthetic strategies to bicyclic tetraphosphanes using P_1, P_2 and P_4 building blocks†

Jonas Bresien,[a] Kirill Faust,[a] Christian Hering-Junghans,[a] Julia Rothe,[a] Axel Schulz*[a,b] and Alexander Villinger[a]

Received 20th July 2015,
Accepted 28th August 2015

DOI: 10.1039/c5dt02757h

www.rsc.org/dalton

Different reactions of Mes* substituted phosphanes (Mes* = 2,4,6-tri-*tert*-butylphenyl) led to the formation of the bicyclic tetraphosphane Mes*P_4Mes* (**5**) and its unknown Lewis acid adduct **5**·$GaCl_3$. In this context, the *endo–exo* isomer of **5** was fully characterized for the first time. The synthesis was achieved by reactions involving "self-assembly" of the P_4 scaffold from P_1 building blocks (*i.e.* primary phosphanes) or by reactions starting from P_2 or P_4 scaffolds (*i.e.* a diphosphene or cyclic tetraphosphane). Furthermore, interconversion between the *exo–exo* and *endo–exo* isomer were studied by ^{31}P NMR spectroscopy. All compounds were fully characterized by experimental as well as computational methods.

Introduction

Ring systems composed of group 15 elements (pnictogens, Pn) are an intriguing and widely investigated aspect of main group chemistry.[1–3] Within this field of research, the chemistry of phosphorus based ring systems has become an important branch of inorganic chemistry,[4,5] especially in view of the fact that various phosphorus ring systems can be obtained by direct activation of white phosphorus.[6–8] A lot of work has been carried out to improve the selectivity of these activation processes, involving functionalization of P_4 by Lewis acids and bases, (transition) metals, radicals, or singlet carbenes such as N-heterocyclic carbenes (NHCs) or cyclic alkylaminocarbenes (CAACs).[9–12]

Among a plethora of structural motifs found in phosphorus ring systems, the simple tetraphosphabicyclo[1.1.0]butane scaffold (**A**, Scheme 1) is of special interest. Firstly, it can formally be derived from tetrahedral P_4 by "simple" cleavage of one PP bond. Secondly, and more importantly, tetraphosphabicyclo[1.1.0]butanes were indeed obtained by P_4 activation, thus representing worthwhile target molecules in phosphorus chemistry.

The first tetraphosphabicyclo[1.1.0]butane, $(Me_3Si)_2N–P_4–N(SiMe_3)_2$ (**1a**, **1b**, Scheme 2), was synthesized by the group of Niecke in 1982.[13] It was derived from P_2 building blocks utilizing PP coupling reactions. In the following years, some more examples emerged that were derived from P_2 or P_3 units, as reported by Cowley (**2**),[14] Schmidpeter (**3**),[15] Jutzi (**4–6**),[16–19] Weber (**5a**),[20] and Romanenko (**5a**).[21] However, the majority of bicyclic tetraphosphanes was synthesized by P_4 activation, the first example being *exo–exo*-Mes*P_4Mes* (**5a**, Mes* = 2,4,6-tri-*tert*-butylphenyl), which was reported by Fluck and co-workers in 1985.[22,23] Improvement of P_4 activation methods led to various other bicyclic P_4 species, which can be categorized by the aforementioned types of P_4 activation (Scheme 2); important contributions were made by the groups of Baudler (**7**, **8**),[24,25] Power (**9–10**),[26,27] Krossing (**11**),[28] Weigand (**12–15**)[29,30] Tamm (**16**),[31] Roesky and Stalke (**17**),[32] Lappert (**18**),[33] Masuda (**19**),[34] Scheer (**20**, **21**),[10] Karaghiosoff (**22**),[35] Lammertsma (**23–25**),[12] and Jones (**26**).[36] Additionally, various examples of transition metal complexes that incorporate bicyclic P_4 scaffolds were reported.[11,37–42] In contrast, very few examples of self-assembly reactions exist (*i.e.* the bicyclic P_4 scaffold is built from P_1 building blocks in a single reaction); literature reports include Wiberg's $(t\text{-Bu})_3Si–P_4–Si(t\text{-Bu})_3$ (**27**)[43] and Weigand's $[Ph_3Pn–P_4–PnPh_3]^{2+}$ (**28**, Pn = P, As).[44] Just recently, we reported on the cation $[Mes^*P_4(Cl)Mes^*]^+$ (**29**),[45] which in itself was not derived by a self-assembly reaction, but its cyclic P_4 precursor was.[46]

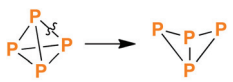

A

Scheme 1 Breaking one of the PP bonds in tetrahedral P_4 formally yields the tetraphosphabicylco[1.1.0]butane scaffold (**A**).

[a]*Institut für Chemie, Universität Rostock, Albert-Einstein-Straße 3a, D-18059 Rostock, Germany. E-mail: axel.schulz@uni-rostock.de*
[b]*Leibniz-Institut für Katalyse e.V. an der Universität Rostock, Albert-Einstein-Straße 29a, D-18059 Rostock, Germany*

†Electronic supplementary information (ESI) available: Experimental and computational details, crystallographic and spectroscopic data. CCDC 1413820–1413827. For ESI and crystallographic data in CIF or other electronic format see DOI: 10.1039/c5dt02757h

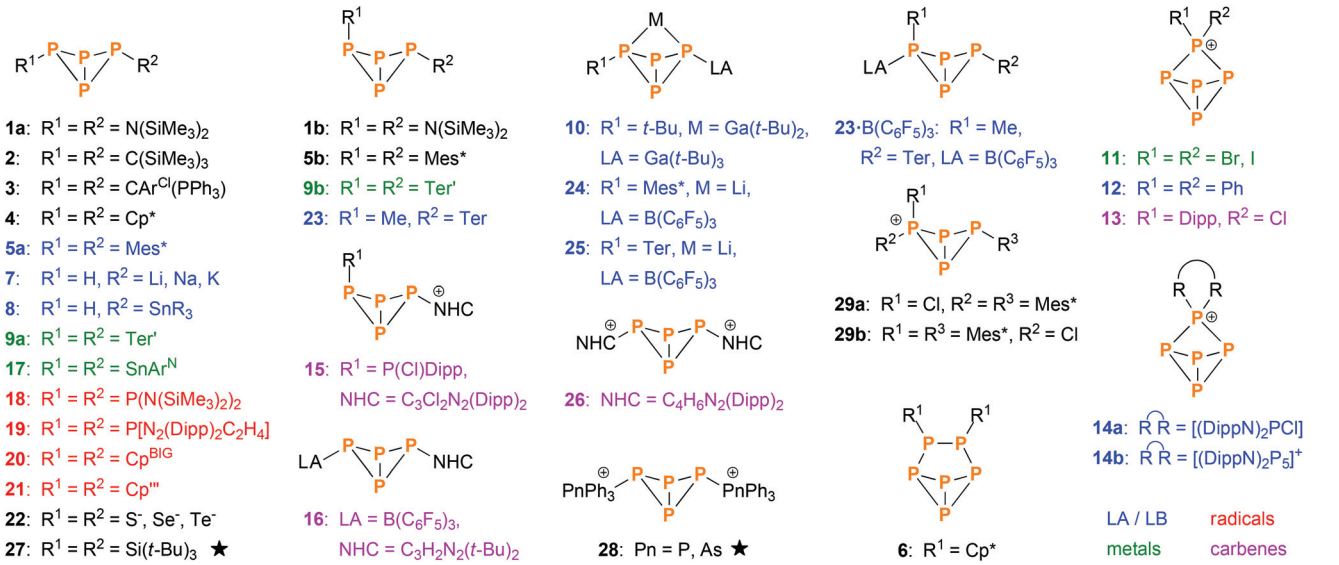

Scheme 2 Overview of known bicyclic tetraphosphane species (not including transition metal complexes). Most were synthesized by direct activation of P_4 using Lewis acids and bases (blue), metals or metal fragments (green), radical species (red) or singlet carbenes (violet). The rest was derived from other precursors, mainly P_2 and P_4 building blocks. Species indicated by a star were derived directly from P_1 building blocks in a self-assembly reaction. Ar^{Cl} = 2,6-dichlorophenyl; Ar^{N} = C_6H_3-2,6-(C(NDipp)CH_3)$_2$; Cp = cyclopentadienyl; Cp* = pentamethyl-Cp; Cp''' = 2,3,5-tri-*tert*-butyl-Cp; Cp^{BIG} = pentakis(4-*n*-butylphenyl)-Cp; Dipp = 2,6-diisopropylphenyl; SnR_3 = $SnMe_3$, $SnPh_3$, Sn(*c*-Hex)$_3$ or Sn(*o*-Tol)$_3$; Ter = 2,6-dimesitylphenyl; Ter' = 2,6-bis(diisopropylphenyl)phenyl; LA = Lewis acid, LB = Lewis Base, NHC = N-heterocyclic carbene.

Interestingly, *exo–exo*-substituted tetraphosphabicyclo-[1.1.0]butanes are considerably more common than their *endo–exo*-substituted counterparts, indicating that the latter are energetically less favoured. We therefore took interest in the synthesis and characterization of rare *endo–exo*-substituted derivatives, which could be synthesized from P_1, P_2 and P_4 building blocks and were analysed by experimental and computational methods.

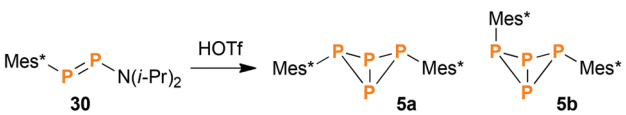

Scheme 3 Reaction of diphosphene **30** with HOTf, yielding bicyclic phosphanes **5a** and **5b** as main products.

Results and discussion

Synthesis and characterization of *endo–exo*-Mes*P_4Mes* (5b)

During our research in functionalized *cyclo*-tetraphosphanes,[46] we came across a publication of Romanenko *et al.*,[21] wherein the authors described the synthesis of *exo–exo*-Mes*P_4Mes* (**5a**) and the asymmetrically substituted bicyclic system Mes*P_4N(i-Pr)$_2$ by reacting the diphosphene Mes*PPN(i-Pr)$_2$ (**30**) with equimolar amounts of HOTf (Tf = SO_2CF_3). Intrigued by this curious method to synthesize bicyclic tetraphosphanes, we tried to reproduce the experiment described in the publication. However, fractional crystallization of the product mixture did not yield the reported compound Mes*P_4N(i-Pr)$_2$, but rather *endo–exo*-Mes*P_4Mes* (**5b**, Scheme 3), alongside the known product **5a** and minor amounts of the diphosphene Mes*PPMes* (**31**).[47,48] Probably the available NMR and MS data were misinterpreted in the original publication. Compound **5b** was now fully characterized for the first time, including NMR, Raman and IR spectroscopy, mass spectrometry, and single crystal X-ray diffraction.

Spectroscopic characterization

Apart from minor impurities, the ^{31}P NMR spectrum of the reaction mixture showed an A_2X_2 (−273.2, −128.3 ppm) and an A_2MX spin system (−220.4, −94.8, −54.7 ppm) in a ratio of 1 : 4. The former set of signals was assigned to **5a** (17% yield based on ^{31}P NMR integrals), the latter to **5b** (67%); hence, the *endo–exo*-isomer was actually formed in significant excess. The same NMR data were obtained for pure **5a** and **5b** (Fig. 1), which agree well with calculated NMR shifts and coupling constants (ESI†) as well as previously reported NMR data.[17,22] Moreover, both isomers could be nicely distinguished in the Raman spectrum due to different excitation energies of the vibrational "breathing" mode of the P_4 scaffold (Table 1). The corresponding Raman bands were easily identified as the most intense signals in both spectra (**5a**: 592 cm^{-1}, **5b**: 568 cm^{-1}). The wavenumbers compare well to the symmetrical A_1 mode of tetrahedral P_4 in the gas phase (600 cm^{-1}).[49] In case of **5b**, two distinct P–C valence modes were identified at 584 (*exo*) and 591 cm^{-1} (*endo*). In **5a**, the single P–C valence band was superimposed by the "breathing" mode of the bicyclic scaffold and could not be discerned.

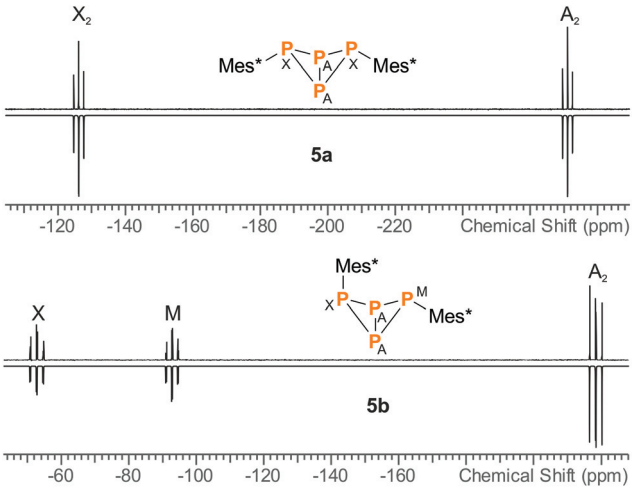

Fig. 1 Experimental (up) and simulated (down) ^{31}P NMR spectra of **5a** and **5b**.

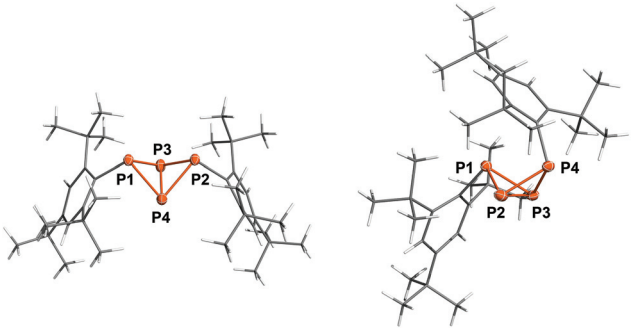

Fig. 2 Molecular structure of **5a** (left) and **5b** (monoclinic, right). Ellipsoids are set at 50% probability (173 K). Selected bond lengths [Å] and angles [°]: **5a** P1–P3 2.2310(7), P1–P4 2.2171(7), P2–P3 2.2294(7), P2–P4 2.2236(7), P3–P4 2.1634(8); P1–P3–P4–P2 −95.66(3); **5b** P1–P2 2.2244(7), P1–P3 2.2326(8), P2–P4 2.2131(8), P3–P4 2.2101(8), P2–P3 2.1773(8); P1–P2–P3–P4 107.78(3).

Molecular structure

Crystallization from *n*-hexane yielded single crystals of **5b** in the space group $P\bar{1}$ while crystallization from CH_2Cl_2 afforded crystals in the space group $P2_1/n$ (Fig. 2, right). The P–P and P–C bond lengths are similar in both modifications of **5b**: the P1–P2 and P1–P3 bonds (av. 2.227, 2.233 Å) are close to the sum of the covalent radii ($\sum r_{cov}$ = 2.22 Å),[50] whereas the P2–P4 and P3–P4 bonds (av. 2.213, 2.210 Å) as well as the transannular bond P2–P3 (av. 2.177 Å) are slightly shorter. This is in contrast to the structure of the previously reported *exo–exo*-isomer **5a** (Fig. 2, left),[22] where all four peripheral P–P bonds exhibit similar lengths (av. 2.225 Å); the transannular bond, however, is likewise only 2.1634(8) Å. The bond angles at the P atoms are all close to 60° and thus compare to tetrahedral P_4. Interestingly, the Mes* substituent in **5b** is bent backwards above the P_4 scaffold, so the *p-tert*-butyl group rests on top of the *exo*-Mes* substituent, effectively shielding the top side of the bicyclic ring system. Hence, the fold angle of the butterfly-shaped P_4 scaffold is quite different in all three cases; it varies from 95.66(3)° (**5a**) across 105.75(5)° (triclinic **5b**) to 107.78(3)° (monoclinic **5b**), which can be attributed to Pauli repulsion between the *endo*-substituent and the opposite bridging atom (P1) in case of **5b** as well as packing effects to account for the difference between the two modifications. A similar effect was observed in case of Ter′P_4Ter′ (**9a**, **9b**, Ter′ = 2,6-bis(diisopropylphenyl)phenyl), where the difference between *exo–exo* (92.9°) and *endo–exo*-isomer (108.1°) is even larger.[27]

Table 1 Main vibrational modes of bicyclic tetraphosphanes in the Raman spectrum. Assignment of the symmetries based on approximate C_{2v} symmetry of the P_4 scaffold

Vibration mode	Description	Frequency [cm^{-1}]
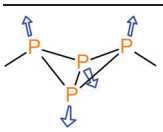	Symmetrical valence "breathing mode" (A_1 mode, in phase)	**5a**: 592 **5b**: 568 **5a**·$GaCl_3$: 597 **5b**·$GaCl_3$: 567
	Peripheral bond stretch (B_1 mode)	**5a**: 447 **5b**: 500 **5a**·$GaCl_3$: 497 **5b**·$GaCl_3$: 518
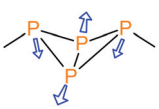	Transannular bond stretch (A_1 mode, out of phase)	**5a**: 412 **5b**: — **5a**·$GaCl_3$: 436 **5b**·$GaCl_3$: —
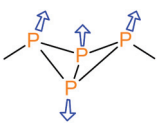	Peripheral bond stretch (B_2 mode)	**5a**: 412 **5b**: 412 **5a**·$GaCl_3$: 451 **5b**·$GaCl_3$: 438

Computational study

Comprehensive DFT calculations were carried out to compare the isomers **5a** and **5b**. According to NBO analysis,[51] the bonding situation is similar in both cases. The Wiberg and NLMO bond indices are near unity for all P–P bonds. However, due to the small bond angles, the electron density is not distributed symmetrically around the P–P bond axes, but rather bent outwards, resulting in banana-shaped bonds. This is illustrated by the electron localization function (ELF, Fig. 3 right), where the local maxima between the P atoms are found outside the lines of nuclear centres. Additionally, the symmetry and shape of the natural bond orbitals (NBOs) and molecular orbitals (MOs) support this picture.

Isomerization of 5b to 5a

At the PBE0/aug-cc-pVDZ level of theory, the *exo–exo*-isomer **5a** is energetically favoured with respect to **5b** by 10.4 kJ mol^{-1} (ΔH^{298}) or 8.80 kJ mol^{-1} (ΔG^{298}), respectively. These findings prompted us to investigate the thermodynamic equilibrium between both isomers: Indeed, when heating a THF solution of **5a** and **5b** (1 : 4 ratio) to 75 °C over a period of 50 days, slow conversion of **5b** to **5a** was observed in the ^{31}P NMR spectrum. The forward and backward reaction were modelled as first order kinetics according to eqn (1).

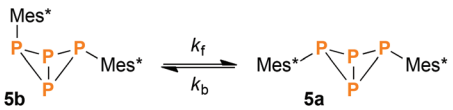

(1)

Hence, eqn (2) defines the reaction rate, [**5a**] and [**5b**] being the partial concentrations of **5a** and **5b**, respectively.

$$\frac{d[\mathbf{5b}]}{dt} = -k_f[\mathbf{5b}] + k_b[\mathbf{5a}] \quad (2)$$

Let $[\mathbf{5a}]_0$ and $[\mathbf{5b}]_0$ denominate the initial concentrations at t = 0. Due to the conservation of mass, $[\mathbf{5b}]_0$–[**5b**] equals [**5a**]–$[\mathbf{5a}]_0$. Furthermore, the reaction rate becomes zero at equilibrium, when the system reaches a steady state with constant concentrations of both isomers. Using these boundary conditions to integrate eqn (2), we obtain

$$[\mathbf{5b}] = c + ([\mathbf{5b}]_0 - c)e^{-(k_f+k_b)t} \quad (3)$$

$$c = \frac{k_b}{k_f + k_b}([\mathbf{5a}]_0 + [\mathbf{5b}]_0) \quad (4)$$

Least-squares fitting of eqn (3) against the experimentally determined concentrations gave k_f = 2.77(11) × 10^{-6} s^{-1} and k_b = 0.30(3) × 10^{-6} s^{-1}. Accordingly, the experimental equilibrium constant is:

$$K = \frac{k_f}{k_b} = 9.3(1.4) \quad (5)$$

Thus, the experimental Gibbs energy (at 75 °C) can be calculated:

$$\Delta_R G = -RT \ln K = -6.4(3) \text{ kJ mol}^{-1} \quad (6)$$

This value compares well to the calculated value of $\Delta_R G^{348}$ = −8.54 kJ mol^{-1} for the gas phase reaction.

Intriguingly, an equilibrium between *endo–exo* and *exo–exo*-isomers was also described for Ter′P$_4$Ter′ (**9a**, **9b**); however, the system was found to be highly dynamic and both isomers afforded identical NMR spectra even at low temperature. Crystallization of either one of the isomers depended solely on the solvent used.[27]

Synthesis of *endo–exo*-Mes*P$_4$Mes* (5b) by carbene promoted degradation of [ClP(μ-PMes*)]$_2$ (32)

Using the synthetic protocol described above, **5a** and **5b** were always obtained in mixture. Separation was difficult and could only be achieved for small amounts of substance by repeated re-crystallization. Designing a reaction that would yield **5b**

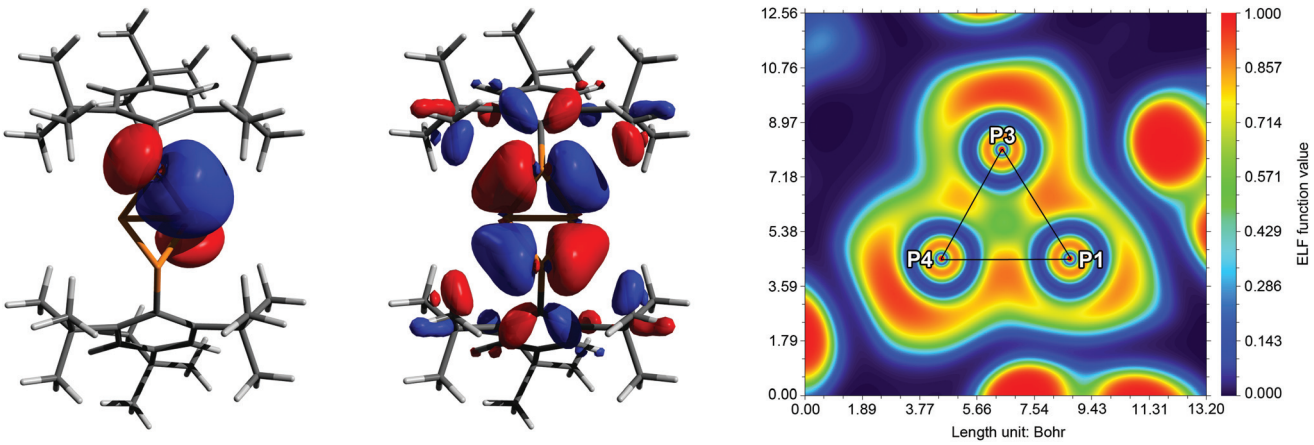

Fig. 3 Exemplary description of the bonding in **5a**. Left: NBO/NLMO depiction of one PP bond, illustrating the "banana" bond character. Middle: HOMO–6 with large coefficients at the central P$_4$ scaffold. Right: Electron localization function (ELF) depicted in a plane through atoms P1, P3 and P4. The maximum densities between the P atoms are found outside the lines of nuclear centres (black). The maxima at the corners of the triangle show the location of the lone pairs (LPs).

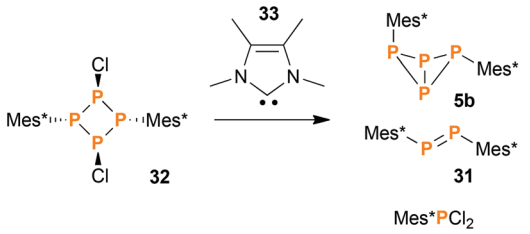

Scheme 4 The carbene promoted degradation of **32** yields a mixture of products, of which some were identified.

exclusively proved to be difficult: obviously, all reactions involving elevated temperatures led to (at least) partial formation of the thermodynamically favoured *exo–exo*-isomer **5a**. Still, we found that the reaction of the *cyclo*-tetraphosphane $[ClP(\mu\text{-}PMes^*)]_2$ (**32**)[46] with tetramethylimidazolylidene (**33**) yielded bicyclic tetraphosphane **5** in a surprisingly good isomeric ratio (**5a** : **5b**) of 1 : 12 (Scheme 4). The isolated yield of pure **5b** was low (14% based on **32**), since the degradation of **32** did not proceed cleanly but rather gave a mixture of different products. Anyway, **5b** could be crystallized from the reaction mixture in large, block-shaped crystals, making isolation comparatively easy.

Selective synthesis of *exo–exo*-Mes*P$_4$Mes* (5a) by reduction

Concerning the synthesis of pure **5a**, the isomerisation at elevated temperatures certainly offered a viable possibility to increase the isomeric ratio in favour of the *exo–exo* isomer. Nevertheless, we found a much more straightforward way to synthesize pure **5a**: starting from **32**, reduction with stoichiometric amounts of Mg afforded **5a** in high yields (based on ^{31}P NMR integrals: 95%; isolated substance: 73%) in a clean reaction (Scheme 5, top). For comparison, the original synthesis of **5a** published by Fluck *et al.* afforded the bicyclic phosphane in a yield of only 5.2%.[22] Formally, the reduction of **32** with Mg can be compared to the reduction of dichloro-*cyclo*-diphosphadiazanes, $[ClP(\mu\text{-}NR)]_2$, which results in the formation of *cyclo*-diphosphadiazanediyls, $[P(\mu\text{-}NR)]_2$, provided that the substituent R is bulky enough to prevent dimerization (Scheme 5, bottom).[52] Yet, in contrast to the bicyclic tetraphosphane, the NP species comprise a planar ring system with singlet biradical character, as there is no classical bonding interaction between the transannular P atoms in this case.

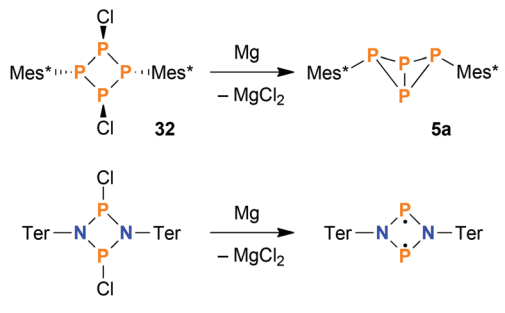

Scheme 5 Top: Reduction of *cyclo*-tetraphosphane **32** yields bicyclic phosphane **5a** selectively. Bottom: Reduction of homologous dichloro-*cyclo*-diphosphadiazanes results in singlet open-shell biradicals with a drastically different bonding situation.

Synthesis of Mes*P$_4$Mes*·GaCl$_3$ (5·GaCl$_3$) from P$_1$ units

When heating a solution of $Mes^*P(SiMe_3)_2$ (**34**) in the presence of PCl_3, a mixture of various products was obtained. Interestingly, the *exo–exo*-isomer **5a** was found to be one of the major products. Other species that could be identified were Mes*PPMes* (**31**), Mes^*PCl_2, P_4, *endo–exo*-isomer **5b** (minor amounts), and some higher aggregates of uncertain composition. However, the reaction was rather slow, so we decided to add a Lewis acid for activation purposes. Indeed, in the presence of $GaCl_3$, complete conversion was detected after one hour even at low temperatures (Scheme 6). Upon slow warming to ambient temperature, colourless crystals of **5a**·$GaCl_3$ or **5b**·$GaCl_3$ were obtained. Depending on the solvent, either one could be crystallized selectively, even though the ratio of both isomers in solution (7 : 5) remained unaffected by the choice of solvent.

Spectroscopic characterization

For both **5a**·$GaCl_3$ and **5b**·$GaCl_3$, an A_2MX spin system was expected due to unsymmetrical substitution of the bicyclic scaffold. Nonetheless, the room temperature ^{31}P NMR spectrum of **5a**·$GaCl_3$ only displayed two resonances (formal A_2X_2 pattern; −246.4, −97.1 ppm; Fig. 4), which were shifted downfield by *ca.* 30 ppm with respect to non-coordinating **5a**. At −80 °C, though, the actual A_2MX spin system was resolved (−248.1, −114.0, −74.8 ppm), with a rather large $^2J_{MX}$ coupling constant of +225 Hz (*cf.* **5b**: $^2J_{MX}$ = −27 Hz). To investigate the nature of this dynamic effect, temperature dependent NMR spectra were recorded. Basically, either an *intra*molecular or an *inter*molecular exchange (*i.e.* dissociation or bimolecular exchange) of the $GaCl_3$ unit could be responsible for the observed line shapes, given that the concentration of free **5a** is much lower than the concentration of the adduct **5a**·$GaCl_3$ (approx. ratio of 10^{-2} or less). However, at such low concentrations, the free phosphane could well be below the detection limit and it might not be discernible in the spectrum even at slow exchange. Accordingly, we added an excess of **5a**, so the appearance of the NMR spectrum would change drastically if the free phosphane (*i.e.* dissociation) was involved in the

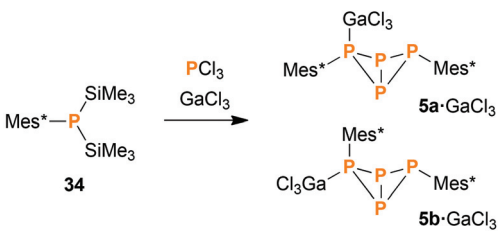

Scheme 6 Reacting **34** with PCl_3 and $GaCl_3$ leads to $GaCl_3$ adducts of the bicyclic tetraphosphane **5**, among other products.

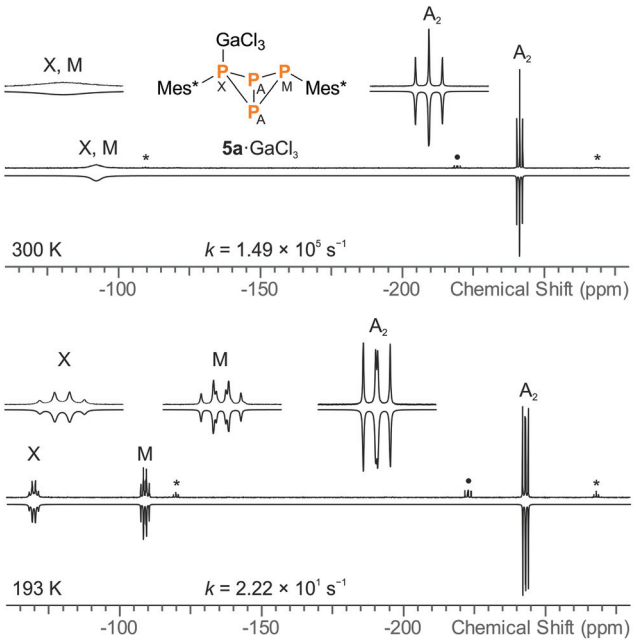

Fig. 4 Experimental (up) and simulated (down) ^{31}P NMR spectra of **5a**·$GaCl_3$ at 27 °C (top) and −80 °C (bottom), demonstrating the dynamic exchange of the $GaCl_3$ moiety in solution (* = **5a**, • = impurity of **5b**·$GaCl_3$). $GaCl_3$ was added to **5a** in slightly sub-stoichiometric amounts (0.95 eq.) so the non-coordinating bicyclic phosphane was detectable in the NMR spectrum.

observed exchange.[53] However, the signals of the excess phosphane could be detected independently of those of the adduct and the signal pattern of **5a**·$GaCl_3$ remained unchanged, regardless of the excess of phosphane, proving an intramolecular mechanism (Scheme 7). Still, at higher temperatures above the coalescence of the M and X signal of **5a**·$GaCl_3$, slight broadening of the signals of free **5a** was detected, hinting at an independent intermolecular exchange. Full lineshape analysis of the NMR signals (Fig. 4, ESI†) facilitated derivation of the rate constants k at different temperatures. Using the Eyring eqn (7), the Gibbs energy of activation of the intramolecular exchange could be determined.

$$k = \kappa \frac{k_B T}{h} \exp\left(-\frac{\Delta G^{\ddagger}}{RT}\right) \quad (7)$$

Least-squares fitting gave a mean Gibbs energy of activation $\Delta G^{\ddagger}$ = 39.5(4) kJ mol^{-1}, which compares, for example, to the activation barrier of the exchange of NH_3 in H_3N·$GaMe_3$ (35.6 kJ mol^{-1}).[54] According to the linearized Eyring plot, the enthalpy of activation $\Delta H^{\ddagger}$ was found to be 39.5(4) kJ mol^{-1} and the entropy of activation $\Delta S^{\ddagger}$ = −0.20(2) J mol^{-1} K^{-1}, indicating a monomolecular transition state in agreement with the discussed intramolecular exchange reaction. The NMR data at slow exchange (−80 °C) correspond well with calculated NMR shifts and coupling constants (ESI†).

The *endo–exo* isomer **5b**·$GaCl_3$ showed an A_2MX spin system (−224.5, −114.5, −50.0 ppm), which resembled the NMR spectrum of free **5b**. Like in **5a**·$GaCl_3$, the A part was broadened due to coupling with Ga. Owing to the arrangement of the Mes* substituents, no intramolecular exchange was observed; the linewidths did not change significantly upon cooling to −80 °C. Nonetheless, upon addition of an excess of **5b** the ^{31}P NMR spectrum revealed a dynamic exchange between free phosphane and adduct, which is most likely caused by a bimolecular exchange of the type **5**·$GaCl_3$ + **5′** ⇌ **5′**·$GaCl_3$ + **5** (ESI†).

Both isomers were nicely distinguishable in the solid state Raman spectra, due to the different positions of the "breathing mode" bands, similar to the non-coordinating tetraphosphabicyclo[1.1.0]butanes **5a** and **5b**. In contrast to the latter, the most intense Raman signal was caused by the Ga–Cl stretching at 343 (**5a**·$GaCl_3$) or 348 cm^{-1} (**5b**·$GaCl_3$). P–C valence modes could be identified at 613 (Mes* at coordinating P, **5a**·$GaCl_3$) and 618 cm^{-1} (*endo*-Mes*, **5b**·$GaCl_3$), the other ones were superimposed by the intense "breathing mode" signals. Important vibrational modes of the P_4 scaffold are summarized in Table 1.

Molecular structure

Lewis acid adduct **5a**·$GaCl_3$ crystallized in the orthorhombic space group *Pnma* as *n*-hexane solvate (Fig. 5). The PP bond lengths lie within the range of typical single bonds, however the P3–P2 (or P3–P2′) bond is slightly shortened (2.1805(9) Å); therefore, the bicyclic structure with two longer and two shorter bonds actually resembles the bicyclic scaffold in **5b**.

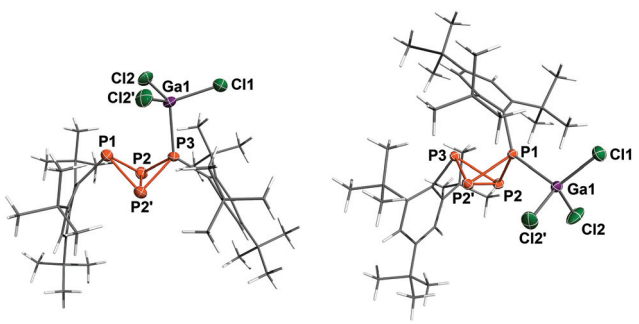

Fig. 5 Molecular structure of **5a**·$GaCl_3$ (left) and **5b**·$GaCl_3$ (right). Ellipsoids are set at 50% probability (173 K). Selected bond lengths [Å] and angles [°]: **5a**·$GaCl_3$ P1–P2 2.228(1), P2–P3 2.1805(9), P2–P2′ 2.200(1), Ga1–P3 2.4206(8); P1–P2–P2′–P3 98.96(3); **5b**·$GaCl_3$ P1–P2 2.1854(5), P2–P3 2.2365(6), P2–P2′ 2.2074(8), P1–Ga1 2.3966(5); P1–P2–P2′–P3 102.64(2).

Scheme 7 In case of **5a**·$GaCl_3$, a fast intramolecular exchange of the $GaCl_3$ unit was observed. The Gibbs energy of activation for this process was determined to be 39.5 kJ mol^{-1}.

The transannular bond (P2–P2′: 2.200(1) Å), on the other hand, is noticeably longer than in **5a** or **5b**. In comparison with the sum of covalent radii (2.35 Å),[50] the P3–Ga1 bond is somewhat elongated (2.4206(8) Å), most likely due to Pauli repulsion between the *ortho-tert*-butyl groups of the neighbouring Mes* moiety and the $GaCl_3$ unit. The bonding angles at the coordinating P atom (P3) are considerably flattened, so one of the Mes* substituents is bent further outwards. Moreover, the fold angle of the bicyclic system amounts to 98.69(3)° and is therefore 3° larger than in **5a**.

Compound **5b**·$GaCl_3$ crystallized in the monoclinic space group $P2_1/m$ either as toluene or CH_2Cl_2 solvate with similar cell parameters and molecular structure. Hence only the toluene solvate shall be discussed in the following: again, the bonds between the bridgehead atoms and the coordinating P atom (P2–P1 and P2′–P1: 2.1854(5) Å) are shortened in comparison with **5b**, whereas the transannular bond is somewhat widened (P2–P2′: 2.2074(8) Å). The P–Ga bond length (2.3699(5) Å) is shorter than in **5a**·$GaCl_3$ and compares well to the sum of covalent radii. The angle of the P3–P2–P2′ plane to the P3–C13 bond axis (96.92(6)°) is about 8° smaller than in **5b**, so the Mes* substituent moves closer to the bicyclic scaffold. In contrast to **5a**·$GaCl_3$, the fold angle of **5b**·$GaCl_3$ lessens with respect to the free bicyclic tetraphosphane by 3° (102.64(2)°).

In both isomers, the substitution pattern at the bicyclic P_4 scaffold is comparable to the borane adduct $TerP_4Me{\cdot}B(C_6F_5)_3$ (**23**·$B(C_6F_5)_3$) or the bicyclic phosphino-phosphonium cation $[Mes^*P_4(Cl)Mes^*]^+$ (**29**).[12,45]

Computational study

NBO analysis revealed that the partial charges of the P atoms in **5a**·$GaCl_3$ and **5b**·$GaCl_3$ (bridgehead P: +0.10*e*, coordinating P: +0.24*e*, non-coordinating P: +0.31*e*) changed only slightly in comparison with **5a** and **5b** (bridgehead P: 0.00*e*, P(Mes*): +0.27*e*), implying a similar distribution of the electron density. Inspection of the molecular orbitals (MOs) showed that the principal bonding orbitals of the P_4 scaffold remained intact. According to the electron localization function (ELF), the P–Ga bond is strongly polarized towards phosphorus (Fig. 6). The natural Lewis description actually suggests a non-bonding situation with a lone pair (LP) at phosphorus and an empty p-type orbital at Ga, with low P–Ga bond indices (NLMO: 0.34, Wiberg: 0.50). However, a second order perturbation analysis revealed a strong donor–acceptor interaction between the LP at P and the empty p-type orbital at Ga (**5a**·$GaCl_3$: 530.5 kJ mol^{-1}, **5b**·$GaCl_3$: 555.2 kJ mol^{-1}); thus, the P–Ga bonding can be described as a classical dative bond. At the PBE0/aug-cc-pVDZ level of theory, the *exo–exo* isomer **5a**·$GaCl_3$ was calculated to be energetically favoured by 8.03 kJ mol^{-1} (ΔG^{298}); therefore the energetic difference between *exo–exo* and *endo–exo*-isomer slightly decreased in comparison to non-coordinating **5a** and **5b**. This is reflected in the calculated Gibbs energies ($\Delta_R G^{298}$) for the association of **5a** or **5b** and $GaCl_3$, which amount to −46.7 kJ mol^{-1} or −47.4 kJ mol^{-1}, respectively.

Equilibrium between 5a·$GaCl_3$ and 5b·$GaCl_3$

Similar to the free phosphanes, the $GaCl_3$ adducts **5a**·$GaCl_3$ and **5b**·$GaCl_3$ were found to interconvert slowly in solution at ambient temperature. Over a period of several weeks, the establishment of equilibrium was monitored by ^{31}P NMR spectroscopy. Interestingly, the equilibrium constant was found to be 1.6(2), thus the amount of *endo–exo* isomer at equilibrium was significantly higher than in case of the free phosphanes. This is in agreement with the calculations, although the actual effect is even more pronounced. According to the experiment, the energetic difference between both isomers is just 1.2(4) kJ mol^{-1} (ΔG).

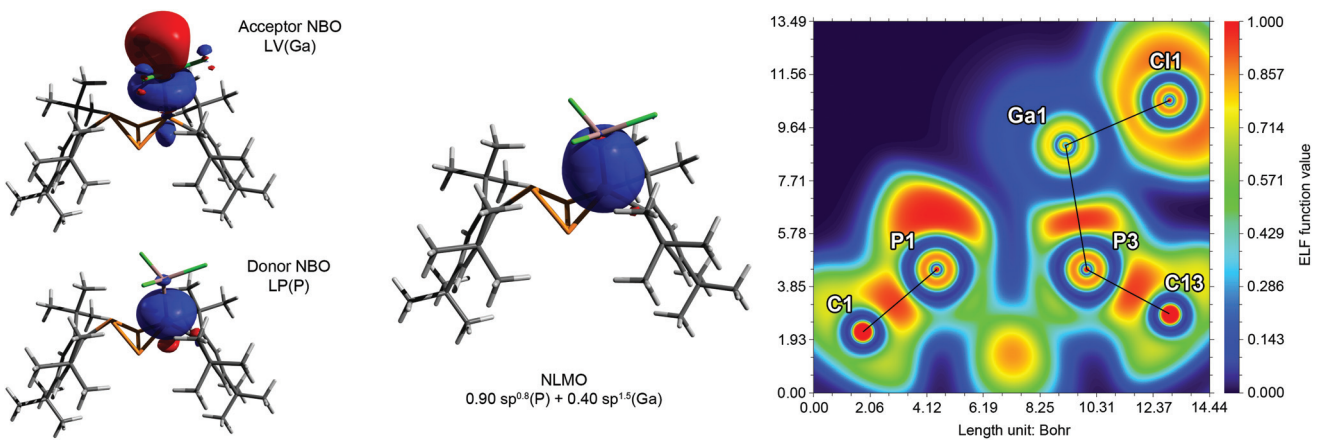

Fig. 6 Exemplary description of the bonding in **5a**·$GaCl_3$. Left: Donor and acceptor NBOs describing the dative bond from P to Ga. Middle: P–Ga bond in the natural localized MO (NLMO) picture. Right: Electron localization function (ELF) depicted in a plane through atoms P1, P3 and Ga1. The P–Ga and Ga–Cl bonds are strongly polarized and exhibit partly ionic character. The deformation of the LP at P1 is due to Pauli repulsion with Cl2 and Cl2′ (out of plane).

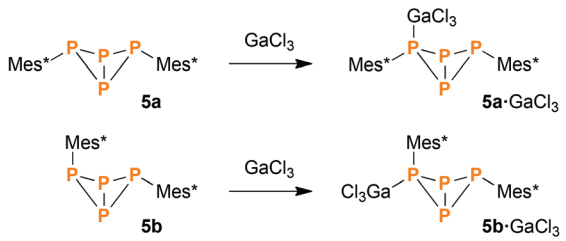

Scheme 8 Rational synthesis of **5a**·$GaCl_3$ and **5b**·$GaCl_3$.

Direct synthesis of Mes*P_4Mes*·$GaCl_3$ (5·$GaCl_3$)

As expected, **5a**·$GaCl_3$ and **5b**·$GaCl_3$ could be synthesized from pure **5a** and **5b** by treatment with equimolar amounts of $GaCl_3$. Mixing solutions of both reactants and subsequent evaporation of the solvent led to quantitative yield of the respective $GaCl_3$ adduct (Scheme 8). Due to the short reaction time (*ca.* 5 min), isomerization could be avoided.

Conclusions

We present new insights into the chemistry of tetraphosphabicyclo[1.1.0]butanes: various synthetic approaches were investigated, involving precursor molecules with one, two or four phosphorus atoms. Thereby, the *endo–exo* isomer of Mes*P_4Mes* (**5b**) could be fully characterized for the first time and the interconversion of both isomers could by studied in detail. Furthermore, the hitherto unknown $GaCl_3$ adducts of both *exo–exo* and *endo–exo* isomer (**5a**·$GaCl_3$, **5b**·$GaCl_3$) were thoroughly investigated, including experimental assessment of dynamic behaviour in solution and computational studies of the bonding situation.

Due to isomerization in solution, it is difficult to obtain either isomer purely; ideally, synthetic strategies should be designed to (a) minimize the reaction time and (b) take place at low temperatures to avoid thermodynamic equilibrium.

Experimental

All manipulations were carried out under oxygen- and moisture-free conditions under argon using standard Schlenk or Drybox techniques. All starting materials containing the Mes* moiety were synthesized according to modified literature procedures; other reactants and solvents were obtained from commercial sources and thoroughly dried. Detailed information concerning experimental procedures, data acquisition and processing, as well as purification of chemicals can be found in the ESI.†

Synthesis of 5a

A solution of $[ClP(\mu\text{-PMes*})]_2$ (206 mg, 0.30 mmol) in THF (3 mL) is added to magnesium turnings (10 mg, 0.42 mmol) and stirred at ambient temperature overnight. Subsequently, the solvent is removed *in vacuo* and the solid residue is extracted with *n*-hexane (5 mL). After filtration, the filtrate is concentrated and stored at 5 °C, resulting in crystallization of colourless *exo–exo*-Mes*P_4Mes*. Yield: 135 mg (0.22 mmol, 73%). CHN calc. (found) in %: C 70.34 (70.32), H 9.51 (9.35). $^{31}P\{^1H\}$ NMR (CD_2Cl_2, 121.5 MHz): δ = −273.2 (t, $^1J_{AX}(^{31}P,^{31}P)$ = −177 Hz, 2 P, $P_{bridgehead}$), −128.3 (t, $^1J_{AX}(^{31}P,^{31}P)$ = −177 Hz, 2 P, *P*Mes*). ^1H NMR (CD_2Cl_2, 300.1 MHz): δ = 1.19 (s, 18 H, *p*-*t*-Bu), 1.63 (s, 36 H, *o*-*t*-Bu), 7.07 (m, 4 H, *m*-H). Raman (633 nm, 15 s, 10 scans, cm^{-1}): $\tilde{\nu}$ = 3075 (1), 2963 (2), 2924 (2), 2903 (3), 2863 (1), 2777 (1), 2709 (1), 1588 (1), 1527 (1), 1473 (1), 1461 (1), 1442 (1), 1396 (1), 1365 (1), 1292 (1), 1281 (1), 1241 (1), 1208 (1), 1201 (1), 1175 (1), 1152 (1), 1128 (1), 1033 (2), 1020 (1), 934 (1), 921 (1), 891 (1), 822 (2), 775 (1), 637 (1), 592 (10), 563 (1), 490 (1), 475 (1), 463 (1), 447 (1), 432 (1), 412 (1), 387 (1), 351 (4), 294 (1), 259 (2), 211 (1), 191 (1), 177 (1), 136 (1), 125 (2), 107 (3), 86 (3).

Synthesis of 5b

Method 1: HOTf (180 mg, 1.12 mmol) is condensed onto a degassed solution of Mes*PPN(i-Pr)$_2$ (489 mg, 1.12 mmol) in CH_2Cl_2 (8 mL) at −196 °C. The reaction mixture is slowly warmed to ambient temperature overnight. The solvent is removed *in vacuo* and the residue is extracted with *n*-hexane (5 mL). Insoluble solids are filtered off. The clear orange filtrate is concentrated, resulting in crystallization of a mixture of *exo–exo* and *endo–exo*-Mes*P_4Mes* (1 : 4 ratio). Yield: 120 mg (0.20 mmol, 35%). Re-crystallization yields pure *endo–exo*-Mes*P_4Mes*. Method 2: A mixture of $[ClP(\mu\text{-PMes*})]_2$ (835 mg, 1.22 mmol) and $Me_4C_3N_2$ (302 mg, 2.44 mmol) is dissolved in CH_2Cl_2 (10 mL) at −80 °C, resulting in a dark red solution. The reaction vessel is warmed to ambient temperature over a period of one hour, whereupon the solution is concentrated and stored at 5 °C, resulting in the crystallization of orange, block shaped crystals that were identified as Mes*PPMes*. The supernatant is separated and concentrated. Storage at 5 °C affords large colourless crystals of *endo–exo*-Mes*P_4Mes*. Yield: 105 mg (0.17 mmol, 14%). CHN calc. (found) in %: C 70.34 (70.04), H 9.51 (9.47). $^{31}P\{^1H\}$ NMR (CD_2Cl_2, 121.5 MHz): δ = −220.4 (dd, $^1J_{AX}(^{31}P,^{31}P)$ = −234 Hz, $^1J_{AM}(^{31}P,^{31}P)$ = −213 Hz, 2 P, P_{bh}), −94.8 (td, $^1J_{AM}(^{31}P,^{31}P)$ = −213 Hz, $^2J_{MX}(^{31}P,^{31}P)$ = −27 Hz, 1 P, P_{exo}), −54.7 (td, $^1J_{AX}(^{31}P,^{31}P)$ = −234 Hz, $^2J_{MX}(^{31}P,^{31}P$ = −27 Hz, 1 P, P_{endo}). ^1H NMR (CD_2Cl_2, 300.1 MHz): δ = 1.19 (s, 9 H, *exo*-Mes*, *p*-*t*-Bu), 1.30 (s, 9 H, *endo*-Mes*, *p*-*t*-Bu), 1.49 (s, 18 H, *exo*-Mes*, *o*-*t*-Bu), 1.66 (m 18 H, *endo*-Mes*, *o*-*t*-Bu), 7.02 (m, 2 H, *exo*-Mes*, *m*-H), 7.05 (m, 2 H, *endo*-Mes*, *m*-H). Raman (633 nm, 15 s, 20 scans, cm^{-1}): $\tilde{\nu}$ = 3168 (1), 3074 (1), 3055 (1), 2959 (4), 2924 (4), 2902 (5), 2865 (2), 2778 (1), 2712 (1), 1584 (3), 1520 (1), 1475 (1), 1466 (2), 1444 (2), 1399 (1), 1392 (1), 1360 (1), 1283 (2), 1251 (1), 1203 (1), 1186 (1), 1182 (1), 1173 (1), 1148 (1), 1132 (2), 1033 (3), 1017 (2), 932 (1), 919 (2), 897 (1), 877 (1), 822 (4), 772 (1), 744 (1), 740 (1), 647 (1), 638 (1), 591 (2), 584 (2), 568 (10), 500 (2), 490 (1), 473 (1), 435 (1), 419 (2), 412 (2), 381 (4), 363 (2), 330 (1),

309 (1), 295 (1), 256 (2), 200 (1), 177 (1), 143 (4), 139 (3), 103 (7), 78 (6).

Synthesis of 5a·$GaCl_3$

Method 1: Solutions of PCl_3 (130 mg, 0.95 mmol) and $GaCl_3$ (168 mg, 0.95 mmol) in *n*-hexane (2 mL each) are added consecutively to a stirred solution of Mes*P$(SiMe_3)_2$ (403 mg, 0.95 mmol) in *n*-hexane (5 mL) at −80 °C. The mixture is warmed to ambient temperature, resulting in the deposition of an intensively red oil. Overnight, large colourless crystals grow at the phase interface at ambient temperature. Yield: 45 mg (0.07 mmol, 8%). Method 2: A solution of $GaCl_3$ (10 mg, 0.057 mmol) in CH_2Cl_2 (1 mL) is added to a solution of *exo–exo*-Mes*P_4Mes* (35 mg, 0.057 mmol) in CH_2Cl_2 (2 mL). The mixture is stirred for ten minutes and the solvent is removed *in vacuo*, yielding an analytically pure powder of *exo–exo*-Mes*P_4Mes*·$GaCl_3$. Yield: 30 mg (0.038 mmol, 67%). CHN calc. (found) in %: C 54.68 (53.97), H 7.39 (6.89). $^{31}P\{^1H\}$ NMR (CD_2Cl_2, 121.5 MHz): δ = −246.4 (t, $^1J_{AX}(^{31}P,^{31}P)$ = −198 Hz, 2 P, $P_{bridgehead}$), −97.1 (broad, 2 P, *P*Mes*). $^{31}P\{^1H\}$ NMR (CD_2Cl_2, 121.5 MHz, −80 °C): δ = −248.1 (dd, $^1J_{AM}(^{31}P,^{31}P)$ = −182 Hz, $^1J_{AX}(^{31}P,^{31}P)$ = −216 Hz, 2 P, $P_{bridgehead}$), −114.0 (dt, $^1J_{AM}(^{31}P,^{31}P)$ = −182 Hz, $^2J_{MX}(^{31}P,^{31}P)$ = +225 Hz, 1 P, *P*Mes*), −74.8 (dt, $^1J_{AX}(^{31}P,^{31}P)$ = −216 Hz, $^2J_{MX}(^{31}P,^{31}P)$ = +225 Hz, 1 P, *P*(Ga)Mes*). ^1H NMR (CD_2Cl_2, 300.1 MHz): δ = 1.20 (s, 18 H, Mes*, *p*-*t*-Bu), 1.68 (s, 36 H, *o*-*t*-Bu), 7.24 (s, 4 H, *m*-H). Raman (785 nm, 30 s, 4 scans, cm^{-1}): $\tilde{\nu}$ = 3064 (1), 2976 (1), 2960 (2), 2928 (2), 2904 (3), 2869 (1), 2786 (1), 2717 (1), 1593 (3), 1582 (2), 1536 (1), 1477 (2), 1465 (3), 1443 (2), 1393 (2), 1362 (1), 1284 (3), 1250 (2), 1208 (2), 1176 (3), 1031 (3), 1025 (3), 1016 (2), 920 (2), 891 (1), 819 (5), 772 (1), 747 (1), 638 (1), 613 (3), 597 (9), 561 (4), 502 (1), 497 (1), 480 (2), 470 (1), 451 (2), 436 (2), 406 (3), 395 (4), 385 (3), 366 (4), 343 (10), 294 (2), 260 (4).

Synthesis of 5b·$GaCl_3$

Method 1: A solution of PCl_3 (131 mg, 0.95 mmol) in CH_2Cl_2 (1 mL) and a solution of $GaCl_3$ (168 mg, 0.95 mmol) in CH_2Cl_2/toluene (1 : 1, 2 mL) are added consecutively to a stirred solution of Mes*P$(SiMe_3)_2$ (403 mg, 0.95 mmol) in CH_2Cl_2 (5 mL) at −80 °C. The mixture is warmed to −50 °C, whereupon the solution turns red. After further stirring at −50 °C for two hours, the solution is concentrated and subsequently warmed to ambient temperature overnight, resulting in crystallization of *endo–exo*-Mes*P_4Mes*·$GaCl_3$ (CH_2Cl_2 solvate) in colourless, block-shaped crystals. The solvent is removed by drying *in vacuo*. Yield: 50 mg (0.08 mmol, 9%). Method 2: A solution of $GaCl_3$ (15 mg, 0.085 mmol) in CH_2Cl_2 (1 mL) is added to a solution of *endo–exo*-Mes*P_4Mes* (52 mg, 0.085 mmol) in CH_2Cl_2 (2 mL). The mixture is stirred for ten minutes and the solvent is removed *in vacuo*, yielding an analytically pure powder of *endo–exo*-Mes*P_4Mes*·$GaCl_3$. Yield: 51 mg (0.064 mmol, 75%). CHN calc. (found) in %: C 54.68 (54.15), H 7.39 (7.15). $^{31}P\{^1H\}$ NMR (CD_2Cl_2, 121.5 MHz): δ = −224.5 (dd, $^1J_{AM}(^{31}P,^{31}P)$ = −192 Hz, $^1J_{AX}(^{31}P,^{31}P)$ = −249 Hz, 2 P, $P_{bridgehead}$), −114.5 (td, $^1J_{AM}(^{31}P,^{31}P)$ = −192 Hz, $^1J_{MX}(^{31}P,^{31}P)$ = +24 Hz, 1 P, P_{exo}), −50.0 (broad, 1 P, P_{endo}). ^1H NMR (CD_2Cl_2, 300.1 MHz): δ = 1.21 (s, 9 H, *exo*-Mes*, *p*-*t*-Bu), 1.33 (s, 9 H, *endo*-Mes*, *p*-*t*-Bu), 1.49 (s, 18 H, *exo*-Mes*, *o*-*t*-Bu), 1.70 (m 18 H, *endo*-Mes*, *o*-*t*-Bu), 7.11 (d, $J(^1H,^{31}P)$ = 1.9 Hz, 2 H, *exo*-Mes*, *m*-H), 7.32 (d, $J(^1H,^{31}P)$ = 5.0 Hz, 2 H, *endo*-Mes*, *m*-H). Raman (633 nm, 10 s, 4 scans, cm^{-1}): $\tilde{\nu}$ = 3055 (2), 3035 (1), 2973 (5), 2966 (6), 2905 (7), 2866 (3), 2782 (1), 2714 (1), 1603 (1), 1582 (4), 1525 (1), 1463 (2), 1441 (2), 1394 (1), 1362 (1), 1284 (2), 1208 (2), 1173 (1), 1133 (2), 1029 (3), 1011 (2), 1002 (3), 924 (1), 818 (3), 784 (2), 741 (2), 618 (3), 567 (7), 518 (1), 508 (1), 438 (3), 407 (2), 391 (2), 372 (2), 348 (10), 302 (1), 258 (3), 213 (1).

Detailed analytical data for all compounds, including low temperature NMR data, can be found in the ESI.†

Acknowledgements

We thank Dr Dirk Michalik for the measurement of low-temperature NMR spectra, Dr Alexander Hinz for a gift of tetramethylimidazolylidene, and the Fonds der Chemischen Industrie (JB) as well as the Deutsche Forschungsgemeinschaft (SCHU 1170/11-1) for financial support.

Notes and references

1 L. Stahl, *Coord. Chem. Rev.*, 2000, **210**, 203–250.
2 M. S. Balakrishna, D. J. Eisler and T. Chivers, *Chem. Soc. Rev.*, 2007, **36**, 650–664.
3 G. He, O. Shynkaruk, M. W. Lui and E. Rivard, *Chem. Rev.*, 2014, **114**, 7815–7880.
4 O. J. Scherer, *Comments Inorg. Chem.*, 1987, **6**, 1–22.
5 M. Baudler and K. Glinka, *Chem. Rev.*, 1993, **93**, 1623–1667.
6 M. Scheer, G. Balázs and A. Seitz, *Chem. Rev.*, 2010, **110**, 4236–4256.
7 B. M. Cossairt, N. A. Piro and C. C. Cummins, *Chem. Rev.*, 2010, **110**, 4164–4177.
8 N. A. Giffin and J. D. Masuda, *Coord. Chem. Rev.*, 2011, **255**, 1342–1359.
9 J. D. Masuda, W. W. Schoeller, B. Donnadieu and G. Bertrand, *Angew. Chem., Int. Ed.*, 2007, **46**, 7052–7055.
10 S. Heinl, S. Reisinger, C. Schwarzmaier, M. Bodensteiner and M. Scheer, *Angew. Chem., Int. Ed.*, 2014, **53**, 7639–7642.
11 S. Heinl and M. Scheer, *Chem. Sci.*, 2014, **5**, 3221–3225.
12 J. E. Borger, A. W. Ehlers, M. Lutz, J. C. Slootweg and K. Lammertsma, *Angew. Chem., Int. Ed.*, 2014, **53**, 12836–12839.
13 E. Niecke, R. Rüger and B. Krebs, *Angew. Chem., Int. Ed. Engl.*, 1982, **21**, 544–545.
14 A. H. Cowley, P. C. Knueppel and C. M. Nunn, *Organometallics*, 1989, **8**, 2490–2492.
15 H.-P. Schrödel, H. Nöth, M. Schmidt-Amelunxen, W. W. Schoeller and A. Schmidpeter, *Chem. Ber.*, 1997, **130**, 1801–1805.
16 P. Jutzi and T. Wippermann, *J. Organomet. Chem.*, 1985, **287**, C5–C7.

17 P. Jutzi and U. Meyer, *J. Organomet. Chem.*, 1987, **333**, C18–C20.
18 P. Jutzi, R. Kroos, A. Müller and M. Penk, *Angew. Chem.*, 1989, **101**, 628–629.
19 P. Jutzi and N. Brusdeilins, *Z. Anorg. Allg. Chem.*, 1994, **620**, 1375–1380.
20 L. Weber, G. Meine, R. Boese and N. Niederprün, *Z. Naturforsch., B: Chem. Sci.*, 1988, **43**, 415–721.
21 V. D. Romanenko, V. L. Rudzevich, E. B. Rusanov, A. N. Chernega, A. Senio, J.-M. Sotiropoulos, G. Pfister-Guillouzo and M. Sanchez, *J. Chem. Soc., Chem. Commun.*, 1995, 1383–1385.
22 R. Riedel, H.-D. Hausen and E. Fluck, *Angew. Chem., Int. Ed. Engl.*, 1985, **24**, 1056–1057.
23 E. Fluck, R. Riedel, H.-D. Hausen and G. Heckmann, *Z. Anorg. Allg. Chem.*, 1987, **551**, 85–94.
24 M. Baudler, C. Adamek, S. Opiela, H. Budzikiewicz and D. Ouzounis, *Angew. Chem., Int. Ed. Engl.*, 1988, **27**, 1059–1061.
25 M. Baudler and B. Wingert, *Z. Anorg. Allg. Chem.*, 1992, **611**, 50–55.
26 M. B. Power and A. R. Barron, *Angew. Chem., Int. Ed. Engl.*, 1991, **30**, 1353–1354.
27 A. R. Fox, R. J. Wright, E. Rivard and P. P. Power, *Angew. Chem., Int. Ed.*, 2005, **44**, 7729–7733.
28 I. Krossing and I. Raabe, *Angew. Chem., Int. Ed.*, 2001, **40**, 4406–4409.
29 M. H. Holthausen and J. J. Weigand, *J. Am. Chem. Soc.*, 2009, **131**, 14210–14211.
30 J. J. Weigand, M. H. Holthausen and R. Fröhlich, *Angew. Chem., Int. Ed.*, 2009, **48**, 295–298.
31 D. Holschumacher, T. Bannenberg, K. Ibrom, C. G. Daniliuc, P. G. Jones and M. Tamm, *Dalton Trans.*, 2010, **39**, 10590–10592.
32 S. Khan, R. Michel, J. M. Dieterich, R. A. Mata, H. W. Roesky, J. P. Demers, A. Lange and D. Stalke, *J. Am. Chem. Soc.*, 2011, **133**, 17889–17894.
33 J.-P. Bezombes, P. B. Hitchcock, M. F. Lappert and J. E. Nycz, *Dalton Trans.*, 2004, 499–501.
34 N. A. Giffin, A. D. Hendsbee, T. L. Roemmele, M. D. Lumsden, C. C. Pye and J. D. Masuda, *Inorg. Chem.*, 2012, **51**, 11837–11850.
35 C. Rotter, M. Schuster and K. Karaghiosoff, *Inorg. Chem.*, 2009, **48**, 7531–7533.
36 A. Sidiropoulos, B. Osborne, A. N. Simonov, D. Dange, A. M. Bond, A. Stasch and C. Jones, *Dalton Trans.*, 2014, **43**, 14858–14864.
37 M. Baudler and B. Wingert, *Z. Anorg. Allg. Chem.*, 1993, **619**, 1977–1983.
38 P. Jutzi, N. Brusdeilins, H.-G. Stammler and B. Neumann, *Chem. Ber.*, 1994, **127**, 997–1001.
39 O. J. Scherer, G. Schwarz and G. Wolmershäuser, *Z. Anorg. Allg. Chem.*, 1996, **622**, 951–957.
40 O. J. Scherer, T. Hilt and G. Wolmershäuser, *Organometallics*, 1998, **17**, 4110–4112.
41 P. Barbaro, C. Bazzicalupi, M. Peruzzini, S. Seniori Costantini and P. Stoppioni, *Angew. Chem., Int. Ed.*, 2012, **51**, 8628–8631.
42 S. Pelties, D. Herrmann, B. de Bruin, F. Hartl and R. Wolf, *Chem. Commun.*, 2014, 7014–7016.
43 N. Wiberg, A. Wörner, H.-W. Lerner and K. Karaghiosoff, *Z. Naturforsch., B: Chem. Sci.*, 2002, **57**, 1027–1035.
44 M. Donath, E. Conrad, P. Jerabek, G. Frenking, R. Fröhlich, N. Burford and J. J. Weigand, *Angew. Chem., Int. Ed.*, 2012, **51**, 2964–2967.
45 J. Bresien, K. Faust, A. Schulz and A. Villinger, *Angew. Chem., Int. Ed.*, 2015, **54**, 6926–6930.
46 J. Bresien, C. Hering, A. Schulz and A. Villinger, *Chem. – Eur. J.*, 2014, **20**, 12607–12615.
47 M. Yoshifuji, I. Shima, N. Inamoto, K. Hirotsu and T. Higuchi, *J. Am. Chem. Soc.*, 1981, **103**, 4587–4589.
48 M. Yoshifuji, I. Shima, N. Inamoto, K. Hirotsu and T. Higuchi, *J. Am. Chem. Soc.*, 1982, **104**, 6167.
49 Y. M. Bosworth, R. J. H. Clark and D. M. Rippon, *J. Mol. Spectrosc.*, 1973, **46**, 240–255.
50 P. Pyykkö and M. Atsumi, *Chem. – Eur. J.*, 2009, **15**, 12770–12779.
51 E. D. Glendening, J. K. Badenhoop, A. E. Reed, J. E. Carpenter, J. A. Bohmann, C. M. Morales, C. R. Landis and F. Weinhold, *NBO 6.0*, Theoretical Chemistry Institute, University of Wisconsin, Madison, 2013.
52 T. Beweries, R. Kuzora, U. Rosenthal, A. Schulz and A. Villinger, *Angew. Chem., Int. Ed.*, 2011, **50**, 8974–8978.
53 H. Schmidbaur, A. Shiotani and H. F. Klein, *J. Am. Chem. Soc.*, 1971, **93**, 1555–1557.
54 J. B. DeRoos and J. P. Oliver, *J. Am. Chem. Soc.*, 1967, **89**, 3970–3977.